Parametric dependence of single-bubble sonoluminescence spectra

G. Simon[1] and M. T. Levinsen[2]
[1]*Department of Atomic Physics, Eötvös Loránd University, H-1117 Budapest, Hungary*
[2]*Complexity Lab, Niels Bohr Institute, Blegdamsvej 17 DK 2100, Copenhagen Ø, Denmark*
(Received 26 April 2003; published 27 October 2003)

We present experimental spectra of single sonoluminescing bubble in water at different dissolved argon concentrations and excitation levels. All the relevant experimental conditions are either measured directly or derived from measured quantities for each spectrum, thus the parametric dependence of the spectra can be analyzed. To characterize the data in a given wavelength interval we fitted the shape of the spectra with the Planck function. The effective temperatures obtained from these fits lie in the range 12 000–18 000 K, practically independent of the expansion ratio, while the intensity normalized by the volume of the bubble increases with the expansion ratio as a power law. The effective temperatures decrease with the pressure amplitude for each argon concentration, while the light intensity, measured with a photomultiplier tube, increases. These observations suggest that the increased energy input due to the higher pressure amplitudes results in an increased number of less energetic photons as compared to the case of a lower excitation level.

DOI: 10.1103/PhysRevE.68.046307 PACS number(s): 78.60.Mq, 43.25.+y, 47.55.Dz

I. INTRODUCTION

Single-bubble sonoluminescence (SBSL) is probably the only ''table-top'' phenomenon, where extreme conditions of high density, pressure, and temperature can be achieved and studied (see Refs. [1,2] for reviews of the phenomenon). These conditions are present inside a tiny bubble that undergoes highly nonlinear volumetric oscillations in response to harmonic acoustic excitation of the surrounding liquid. During SBSL the bubble collapses in each acoustic period close to its van der Waals hard core, and at these instants the compressed hot gas also emits brief flashes of light visible to the eye.

One of the most exciting aspects of SBSL is the spectrum of the emitted radiation. The first measurements of Hiller *et al.* [3] done in the wavelength interval 200–800 nm revealed a continuum spectrum without the presence of characteristic spectral lines of the host liquid or the gas, and with a spectral density increasing strongly towards the ultraviolet region. The experimental spectra could be characterized by fitting their shape with the Planck function. This procedure produced effective temperatures of the order of 10^4 K. In the history of research of SBSL, comparison of experimental spectra to theoretical predictions plays a crucial role in justifying theoretical models. Although relatively many experimental spectra were reported in the literature (see, e.g., Refs. [4,1,5–7]), however, so far in all of these measurements some of the important parameters of the bubble dynamics, pressure amplitude P_a, ambient radius R_0, or the precise experimental conditions were not reported, which gives considerable freedom for the theoretical models to reproduce them. It must be mentioned that measuring the spectrum simultaneously with the dynamical parameters using the conventional methods is not an easy task, since both Mie scattering [8] and direct imaging of the bubble [9] require the disturbing presence of a laser light or back lighting.

In this paper we report a measured spectrum, where the dynamical parameters were deduced from directly measurable quantities using the method of Ref. [10], which avoids the technical difficulties of the previous methods.

II. DESCRIPTION OF THE MEASURING SETUP

In the experiment, the light of the bubble was detected by a photomultiplier tube (PMT) (type: Hamamatsu R3478) and a fiber optic spectrometer (OCEAN OPTICS S2000). We used the same quartz fiber with a diameter of 0.4 mm for all the measurements, including calibration. The acoustic resonator was similar to that described in detail in Ref. [11], with the modification that a hole was drilled in the center of the upper end cap, where the quartz fiber could be immersed in water. This hole was closed with a plug during the water preparation, and the plug was only removed immediately before the start of the spectral measurement to guarantee that the gas concentration in water matched the preset values. The setup is placed in a modified refrigerator to minimize the undesired background light, and to facilitate measurements at reduced temperatures. However, all measurements presented here are performed at an ambient temperature. The water temperature was monitored with a thermocouple (accuracy 0.5 °C), immersed in water through the upper filling tube of the resonator. The position of the PMT and of the quartz fiber was fixed while the resonator was placed on a stand, which could be translated accurately in all directions.

After a light emitting bubble was generated, the position of the resonator was adjusted to ensure that both the PMT and the fiber look directly at the bubble. Right positioning was achieved by connecting the spectrometer end of the fiber to the white light from a tungsten halogen lamp, which produced a clearly visible narrow light cone at the other end. The horizontal position of the resonator was adjusted until the bubble was in the center of the light cone, then the vertical position was set to bring the bubble close to the aperture of the fiber. The distance between the bubble and the fiber was between 1 and 5 mm in all cases, and the distance to the PMT was 50 ± 2 mm.

After positioning, the end of the fiber was removed from the tungsten halogen lamp and connected to the spectrometer. Simultaneous spectral and PMT measurements were taken, and the electric driving signal applied to the piezotransmitters of the resonator was also recorded. This procedure was repeated at different excitation levels and gas concentrations. The role of the PMT in this measurement is binary. First, it provides the timing information needed to deduce the dynamical parameters using the method of Ref. [10]. Second, the recorded light intensity of the bubble was used to normalize each spectrum upto a common multiplicative constant, in order to adjust for different distances between the bubble and the fiber in each case.

A. Calibration procedure

The spectral response of the spectrometer with the fiber was calibrated in two overlapping wavelength intervals by a tungsten halogen light source (OCEAN OPTICS LSC048, calibrated in the interval 350–900 nm) and by a deuterium discharge lamp (Cathodeon Ltd C80-10V-SMFF, calibrated in the interval 115–400 nm), following closely the instructions provided with the instruments during their operation. The resulting relative response of the system is given in Fig. 1(a). It was obtained by dividing the measured intensities $I_m(\lambda)$ with the calibrated intensities $I_c(\lambda)$ tabulated in the manuals of the deuterium and the tungsten halogen lamps. The two response curves were then scaled to provide the same intensities in the overlapping wavelength region 350–400 nm. As can be seen, the spectrometer is most sensitive near ≈500 nm. Because of the relatively big uncertainty in the distances from the bubble to the aperture of the fiber, we did not attempt absolute calibration, thus useful information is contained only in the shape of our final spectra, and in their relative spectral densities.

B. Processing the spectra

Figures 1(b)–1(d) illustrate the steps during which a raw spectrum is transformed into its final form. If no light enters the spectrometer one can record the dark signal. Figure 1(b) shows the dark integrated for 46 ms and averaged over 10 samples (we used these settings to obtain the other spectra as well). It is found to be wavelength dependent, but practically constant with time. In the same figure, above the dark we show a raw SBSL spectrum. The superimposed dark signal can be eliminated by subtraction, which results in a smooth raw spectrum [see Fig. 1(c)]. Since the sensitivity of the spectrometer is wavelength dependent, to correct for this one needs to divide the raw spectra with the response curve in Fig. 1(a), which sets their final shape $[S_i^m(\lambda)]$. Since for each spectrum the distance between the fiber and the bubble is known only with the uncertainty of 1–5 mm, thus the absolute calibration constant A_i for each spectrum is different. One may write this as

$$S_i^c(\lambda) = A_i S_i^m(\lambda), \tag{1}$$

where $S_i^c(\lambda)$ is the ''correct'' spectrum that not only has the same shape as $S_i^m(\lambda)$, but also correct spectral density values at every wavelength. To be able to compare the relative spectral densities of the measured spectra one needs to correct for the effect of the different distances. For this reason we use the amplitude of the recorded PMT signal I_i^{PMT} as giving an intensity proportional to the number of detected photons N_i, determined by the wavelength dependent quantum efficiency of the PMT $Q(\lambda)$ [see the dotted line in Fig. 1(d) taken from the manufacturer's data]:

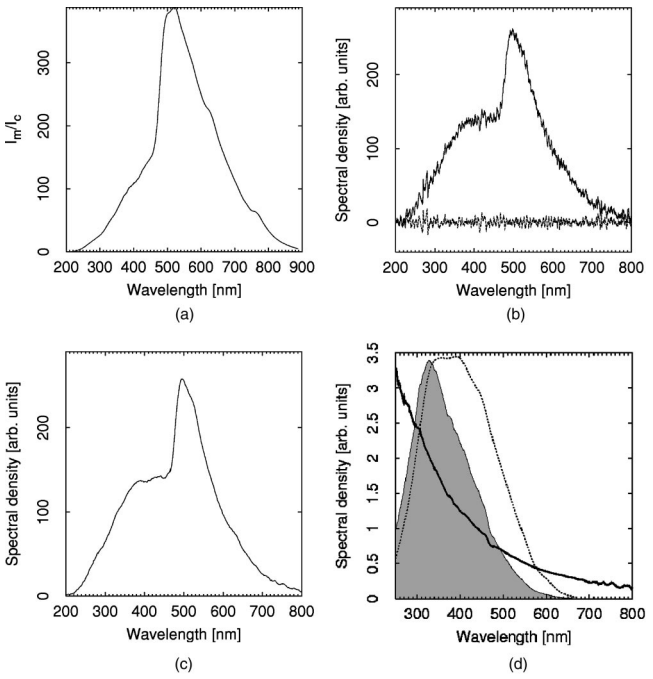

FIG. 1. The relative response of the spectrometer with the fiber as a function of the wavelength (a). Here I_m is the measured intensity and I_c is the intensity according to the calibration data. In (b) the horizontal fluctuating curve is the dark signal of the spectrometer, and the other curve above it is the raw SBSL spectrum. In (c) the raw SBSL spectrum is shown after subtracting the dark. Finally in (d) the dotted curve indicates the quantum efficiency of the PMT that also recorded the light of the bubble, the continuous line is the shape-corrected SBSL spectrum obtained by dividing (c) with (a), and the area of the shaded region is the quantity I^* proportional to the light intensity, which the PMT ''sees'' from the shape-corrected spectrum.

$$I_i^{PMT} = BN_i, \tag{2}$$

where B is a common proportionality constant, which is the same for all spectra since the distance between the bubble and the PMT was essentially constant. To obtain the final corrected spectra we use the following transformation:

$$S_i^f(\lambda) = S_i^m(\lambda)\frac{I_i^{PMT}}{I_i^*}, \tag{3}$$

where I_i^* is defined as

$$I_i^* = \int_{\lambda_1}^{\lambda_2} S_i^m(\lambda) Q(\lambda) d\lambda, \tag{4}$$

with $\lambda_1 = 250$ nm and $\lambda_2 = 800$ nm. Note that I_i^* is a quantity, which is proportional to the signal that the PMT would detect from $S_i^m(\lambda)$. In Fig. 1(d) the corresponding I^* is the area of the shaded region. Similarly from Eq. (1) and the definition of I_i^* one may write

$$CN_i = \int_{\lambda_1}^{\lambda_2} S_i^c(\lambda) Q(\lambda) d\lambda = A_i I_i^*, \tag{5}$$

where C is a proportionality constant. As shown below all the final transformed spectra have the same absolute calibration constant, thus their relative spectral densities can be compared.

$$S_i^f(\lambda) = S_i^m(\lambda) \frac{I_i^{PMT}}{I_i^*} = S_i^m(\lambda) \frac{A_i I_i^{PMT}}{\int_{\lambda_1}^{\lambda_2} S_i^c(\lambda) Q(\lambda) d\lambda}$$

$$= S_i^c(\lambda) \frac{I_i^{PMT}}{CN_i} = S_i^c(\lambda) \frac{B}{C}. \tag{6}$$

III. EXPERIMENTAL RESULTS

During the measurements, the ambient pressure was $P_0 = 1019 \pm 2$ mbars, the excitation frequency was $f = 22\,650$ Hz, and the water temperature was $T_w = 23.5 \pm 1$ °C. We performed measurements at relative argon concentrations of $C_{\mathrm{Ar}}/C_0^{23.5} = 0.001\,95,\ 0.000\,473,\ 0.000\,248$, where C_{Ar} is the dissolved argon concentration that was set during the water preparation, and $C_0^{23.5}$ is the dissolved argon concentration of water at an ambient pressure of 1 atm and a temperature of 23.5 °C (see Ref. [12] for the actual value and temperature dependence of C_0). The desired gas concentration was set using the degassing system and procedure, described in detail in Ref. [11]. Figure 2 shows the spectra recorded at three different argon concentrations and different levels of acoustic excitation. In each part of the figure the excitation amplitude increases from bottom to top.

It is useful to characterize the experimental data with some (any) kind of functional form for comparison purposes. In Fig. 2 the thin continuous lines are the black-body fit for each spectrum.

$$I_b(\lambda) \propto \frac{1}{\exp\left(\frac{hc}{\lambda k T_{eff}}\right) - 1}, \tag{7}$$

where λ is the wavelength in nanometers, $h = 6.626 \times 10^{-34}$ J s is the Planck constant, $c = 3 \times 10^8$ m/s is the speed of light, and $k = 1.38 \times 10^{-23}$ J/K is the Boltzmann constant. We choose the Planck function partly because of its simplicity (characterization of the spectral shape with the effective temperature) and partly because previous authors of experimental papers also used this form, thus admitting the easy comparison with earlier published experimental spectra.

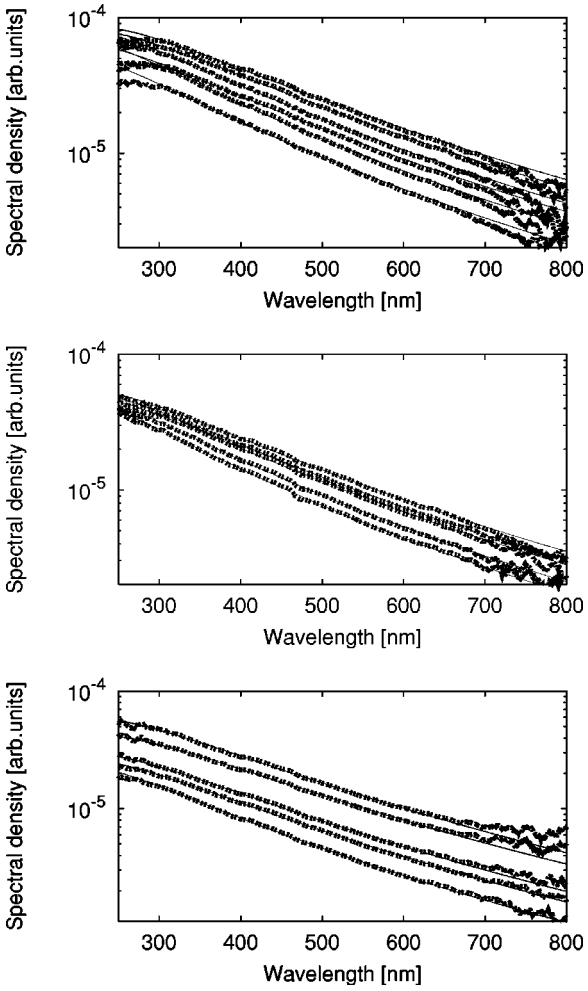

FIG. 2. Experimental spectra (thick dashed lines) and their best blackbody fits (thin continuous lines) at various excitation levels and relative argon concentrations. From top to bottom $C_{\mathrm{Ar}}/C_0^{23.5} = 0.001\,95,\ 0.000\,473,\ 0.000\,248$.

The fitting was made in the wavelength interval 300–700 nm, which is symmetric around $\lambda = 500$ nm, where the sensitivity of our spectrometer is maximal. The best fits provided the values of the effective temperatures T_{eff}.

From the timing information of the flashes and the recorded excitation amplitude on the piezo transmitters, we deduced the pressure amplitude P_a, the ambient radius R_0, and the expansion ratio R_{max}/R_0 for each spectrum using the method of Ref. [10]. The results together with the errors and the best fit effective temperatures are summarized in Table I.

Although the errors of the dynamic parameters are fairly high, nevertheless several interesting trends can still be observed. In Fig. 3 we show the dependence of the effective temperature on the pressure amplitude (a), and expansion ratio (b). The PMT signal amplitude as a function of P_a (c), and the PMT signal amplitude normalized by the ambient volume as a function of the expansion ratio (d) are also shown. A detailed comparison with the most up-to-date theoretical models of SL light emission is outside the scope of the present paper; nevertheless, in the following section we

TABLE I. The parameters of the dynamics and the best fit black-body effective temperatures corresponding to the spectra of Figs. 2. To get a clearer picture, the spectra indicated with * are not shown in Fig. 2.

$C_{Ar}/C_0^{23.5}$	P_a (bars)	R_0 [μm]	R_{max}/R_0	T_{eff} (K)
0.00195	1.345±0.025	4.7±1.1	11.0±3.9	16297±20
	1.376±0.025	5.1±1.2	11.1±3.8	16325±23
	1.400±0.025	5.65±1.3	10.8±3.2	14952±18
	1.400±0.025	5.8±1.3	10.6±3.4	14402±18
	1.431±0.025	5.9±1.35	11.2±3.6	13653±14
	1.446±0.025	6.4±1.43	10.9±3.4	13329±15
0.000473	1.369±0.025	3.53±0.88	13.9±5.1	17052±27
	1.376±0.025	3.38±0.83	14.7±5.2	16274±20
	1.406±0.025	3.43±0.88	15.7±5.9	14574±15
	1.428±0.025	3.4±0.9	16.6±6.5	14432±15
	1.450±0.025	2.7±0.7	20.7±7.8	13914±12
0.000248	1.401±0.025	1.78±0.32	22.9±5.9	15755±19
*	1.401±0.025	2.15±0.55	20.9±6.2	15590±37
*	1.416±0.025	2.43±0.58	20.4±7.0	15197±40
	1.423±0.025	2.6±0.65	19.7±7.2	14130±13
	1.446±0.025	2.53±0.63	21.4±7.7	13786±14
	1.460±0.025	2.4±0.6	23.0±8.4	13022±14
*	1.475±0.025	2.4±0.55	23.8±7.7	13230±27
	1.490±0.025	2.28±0.58	25.3±9.3	13498±19

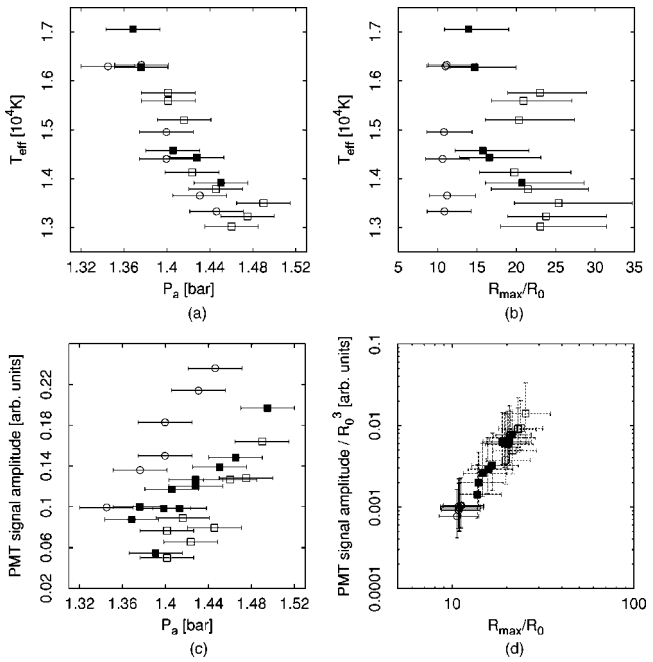

FIG. 3. The parametric dependence of the PMT signal amplitude, and effective temperatures of the measured spectra for dissolved argon concentrations of $C_{\mathrm{Ar}}/C_0^{23.5}=0.001\,95$ (circles), 0.000 473 (filled boxes), 0.000 248 (open boxes).

briefly discuss our results in light of some predictions of theoretical models and compare them to earlier experiments.

IV. DISCUSSION

Looking at Fig. 2 one may notice that at the two lower relative argon concentrations the shape of the spectra are very well reproduced by the simple black-body expression (7), even below 300 nm. However, this should not be construed as a proof that the radiation is indeed from a black-body surface emitter, since there are many possible scenarios that produce a spectrum which is a reminiscent of a black-body in a certain wavelength interval. For instance, Hammer and Frommhold obtains good agreement with experimental data assuming optically thin bubble with a nonuniform heating. (See Fig. 3 in Ref. [18].) Thus the effective temperatures found from the fits should not be interpreted as representing real physical temperatures in the bubble, their purpose is solely to characterize the shape of the spectra in the wavelength interval 300–700 nm through the functional form (7).

At a relative argon concentration of $C_{\mathrm{Ar}}/C_0^{23.5}=0.001\,95$ we find a breakpoint in the spectra at around ≈300 nm, where the spectral density at wavelengths below the breakpoint is less than that of the corresponding black-body fit obtained from the interval 300–700 nm. Although the precision of the spectral density decreases dramatically as the ultra violet (UV) cutoff is approached, at $\lambda=300$ nm the sensitivity of the spectrometer together with the fiber is still around 10% of the maximal value [see Fig. 1(a)], and the error due to the variation of the dark is less than the SBSL signal. This suggests that the observation is due to a real effect and not an artifact of the measurement. Similar qualitative behavior can also be seen in the earlier experiments of Hiller *et al.* [3] and Gaitan *et al.* [4], but in their measurements the breakpoint seems to be around $\lambda\approx250$ nm, and the authors attributed the effect to the UV-cutoff of water.

Moreover, a breakpoint or a maximum point in the spectrum is also one of the predictions of recent theoretical models. Hilgenfeldt *et al.* predict a spectral maximum at $\lambda=294$ nm [see Fig. 4(a) in Ref. [13]] for dynamic parameter values $P_a=1.3$ bars, $R_0=5$ μm, and acoustic frequency $f=20$ kHz, which are quite near to the experimental case corresponding to the first row in Table I. The refined model by Hammer and Frommhold [14] at the same parameter values predicts a breakpoint instead of the maximum (see Fig. 1 in Ref. [15]), which is in excellent qualitative agreement with our measurement. In these theoretical models the discontinuity of the slope in the spectrum arises from the contribution of the electron-ion interaction. Whether the discontinuity manifests itself in a breakpoint or a maximum depends on the contributions from other processes, such as electron-neutral bremsstrahlung, which is more intense in the refined model of Ref. [14]. Given the agreement of the theory and the experiment at these specific parameters, it would be interesting to make comparisons also at the parameter values corresponding to our experiments with lower argon concentrations.

According to the parametric dependence in Fig. 3 the effective temperatures of the data lie in the range between 12 000 and 18 000 K, and decrease with the forcing pressure, while the intensity increases (c). Also the effective temperatures seem to be independent of the expansion ratio (b), while the PMT signal's amplitude normalized by the volume

of the bubble increases as a power law (d). Similar power-law behavior was also found in Ref. [19]. It seems that although more energy can be pumped into the bubble by increasing the pressure amplitude, this input results in an increased number of less energetic photons.

The theoretical models of Refs. [16–18] that incorporate the effect of water vapor predict a narrow range of attainable physical temperatures, basically independent of the expansion ratio, which would likely result in nearly identical spectral shapes in qualitative agreement with our experimental results. This observation confirms the importance of water vapor, whose effect has been investigated experimentally as well as theoretically in several papers (see, for instance, Refs. [20–22]). Its role can be roughly understood if one considers that at higher expansion ratios more vapor gets trapped in the bubble during the collapse. As a result, more energy is taken up by the dissociation of the water molecules and subsequent endothermic reactions of the formed radicals, which counteracts the increased energy input and constrains the maximum attainable temperatures.

V. CONCLUSION

We presented the experimental spectra of SBSL in water at different dissolved argon concentrations and excitation levels. The corresponding parameters of the bubble dynamics, P_a, R_0, and R_{max}/R_0, are deduced for each spectrum using the method of Ref. [10], while all the other relevant ambient conditions are measured, which allows one for a direct comparison with theory. We find that the shape of the spectra can be very well characterized by a simple black-body form in the interval 300–700 nm. At the two lower argon concentrations the agreement between the spectra and the corresponding black-body fits extends down to the lowest measured wavelength, whereas, at the highest argon concentration a breakpoint in the spectral density is observed ($\lambda \approx 300$ nm). In the latter cases, the spectra at wavelengths below the breakpoint start to deviate from the continuation of the black-body fits toward smaller spectral densities. The effective temperatures of the best black-body fits lie in the narrow range 12 000–18 000 K practically independent of the expansion ratio, while T_{eff} is found to decrease with the pressure amplitude for each argon concentration. On the other hand the relative light intensity, as measured by a PMT, increases with P_a, and the same intensity normalized by the volume of the bubble also increases with the expansion ratio. The most likely mechanism responsible for the observed behavior is the effect of water vapor, which also prevented the upscaling of SBSL at reduced excitation frequencies; however, a comparison with detailed theoretical models to confirm this is yet to be done.

ACKNOWLEDGMENTS

The authors acknowledge financial support by the Danish Nonlinear School and the Danish National Science Foundation. G.S. also thanks the ERASMUS for financial support.

[1] B.P. Barber *et al.*, Phys. Rep. **281**, 65 (1997).
[2] M.P. Brenner, S. Hilgenfeldt, and D. Lohse, Rev. Mod. Phys. **74**, 425 (2002).
[3] R.A. Hiller, S.J. Putterman, and B.P. Barber, Phys. Rev. Lett. **69**, 1182 (1992).
[4] D.F. Gaitan, A.A. Atchley, S.D. Lewia, J.T. Carlson, X.K. Maruyama, M. Moran, and D. Sweider, Phys. Rev. E **54**, 525 (1996).
[5] T.J. Matula, R.A. Roy, P.D. Mourad, W.B. McNamara III, and K.S. Suslick, Phys. Rev. Lett. **75**, 2602 (1995).
[6] R.A. Hiller, S.J. Putterman, and K.R. Weninger, Phys. Rev. Lett. **80**, 1090 (1998).
[7] J.B. Young, J.A. Nelson, and W. Kang, Phys. Rev. Lett. **86**, 2673 (2001).
[8] B.P. Barber and S.J. Putterman, Phys. Rev. Lett. **69**, 3839 (1992); W.J. Lentz, A.A. Atchley, and D.F. Gaitan, Appl. Opt. **34**, 2648 (1995).
[9] Y.J. Tian, J.A. Ketterling, and R.E. Apfel, J. Acoust. Soc. Am. **100**, 3976 (1996).
[10] G. Simon and M.T. Levinsen, Phys. Rev. E **67**, 026320 (2003).
[11] G. Simon, Ph.D. thesis, Eötvös University (unpublished); http://www.nbi.dk/~simon/thesis.ps.gz
[12] D.R. Lide, *CRC Handbook of Chemistry and Physics*, 76th ed. (CRC Press, Boca Raton, 1995).
[13] S. Hilgenfeldt, S. Grossmann, and D. Lohse, Phys. Fluids **11**, 1318 (1999).
[14] D. Hammer and L. Frommhold, Phys. Rev. Lett. **85**, 1326 (2000).
[15] D. Hammer and L. Frommhold, Phys. Fluids **12**, 472 (2000).
[16] R. Toegel, B. Gompf, R. Pecha, and D. Lohse, Phys. Rev. Lett. **85**, 3165 (2000).
[17] R. Toegel, S. Hilgenfeldt, and D. Lohse, Phys. Rev. Lett. **88**, 034301 (2002).
[18] D. Hammer and L. Frommhold, Phys. Rev. E **65**, 046309 (2002).
[19] G. Simon, I. Csabai, Á. Horváth, and F. Szalai, Phys. Rev. E **63**, 026301 (2001).
[20] G.E. Vazquez and S.J. Putterman, Phys. Rev. Lett. **85**, 3037 (2000).
[21] B.D. Storey and A.J. Szeri, Proc. R. Soc. London, Ser. A **456**, 1685 (2000).
[22] K. Yasui, Phys. Rev. E **64**, 016310 (2001).